

Symmetry-breaking induced transition among net-zero-magnetization magnets

San-Dong Guo* and Xiao-Shu Guo

School of Electronic Engineering, Xi'an University of Posts and Telecommunications, Xi'an 710121, China

Guangzhao Wang

Key Laboratory of Extraordinary Bond Engineering and Advanced Materials Technology of Chongqing, School of Electronic Information Engineering, Yangtze Normal University, Chongqing 408100, China

Net-zero-magnetization magnets have garnered intensive research attention due to their ultradense and ultrafast potential. In terms of the symmetric classification of connecting magnetic atoms with opposite spin polarization, the net-zero-magnetization magnets mainly include PT -antiferromagnet (the joint symmetry (PT) of space inversion symmetry (P) and time-reversal symmetry (T)), altermagnet and fully-compensated ferrimagnet. Studying transitions among net-zero-magnetization magnets is essentially the research on symmetry breaking, which can also clearly reveal the transformation of spin-splitting symmetry. Symmetry breaking can be achieved through methods such as Janus engineering, isovalent alloying, and external electric field. Here, we start from a parent PT -antiferromagnet that simultaneously possesses both P and rotational/mirror symmetries to induce altermagnet and fully-compensated ferrimagnet. Based on first-principles calculations, the proposed transitions can be verified in PT -antiferromagnet CrC_2S_6 monolayer. By Janus engineering and isovalent alloying, CrC_2S_6 can change into altermagnetic $\text{CrC}_2\text{S}_3\text{Se}_3$ and fully-compensated ferrimagnetic CrMoC_2S_6 . The $\text{CrC}_2\text{S}_3\text{Se}_3$ can also become fully-compensated ferrimagnetic $\text{CrMoC}_2\text{S}_3\text{Se}_3$ by isovalent alloying. Our work provides a clear and intuitive example to explain the transitions among net-zero-magnetization magnets, which can inspire more research on net-zero-magnetization magnets.

Introduction.— Ferromagnets are one of the most important materials in spintronics[1]. The spontaneous magnetization of ferromagnets makes them a stable magnetic storage medium in spintronics. The magnetization direction of ferromagnets can be flipped by an external magnetic field or current, and they are widely used in magnetic random access memory (MRAM) and other storage devices. The ferromagnets can also be used to develop highly sensitive magnetic sensors and readout devices. Although ferromagnets have important applications in spintronics, they also have some limitations: stray field problems and power consumption issues[2–4]. Instead, contemporary interest in spintronics has shifted to net-zero-magnetization magnets. Compared with ferromagnets, net-zero-magnetization magnets offer more advantages for spintronic devices, particularly in terms of high storage density, robustness against external magnetic fields, and ultrafast writing speed, which are all due to their net-zero magnetic moment[2–4]. PT -antiferromagnet (the joint symmetry (PT) of space inversion symmetry (P) and time-reversal symmetry (T)), altermagnet and fully-compensated ferrimagnet are typical net-zero-magnetization magnets[5, 6].

Traditional antiferromagnets, such as PT -antiferromagnet, exhibit spin degeneracy, which limits many interesting physical phenomena and effects. The spin-splitting can be induced by making the magnetic atoms with opposite spin polarization locating in the different environment[7]. That is to say, it is necessary to break the P symmetry of the system[8, 9], and PT -antiferromagnet can become altermagnet and fully-compensated ferrimagnet with

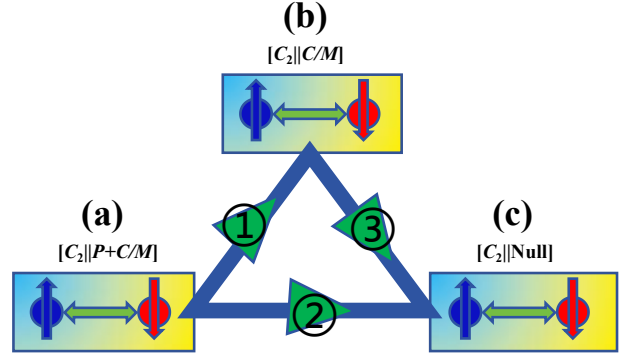


FIG. 1. (Color online) The net-zero-magnetization magnet mainly includes PT -antiferromagnet (a), altermagnet (b) and fully-compensated ferrimagnet (c). The magnetic atoms with opposite spins are connected by inversion symmetry (P), rotation/mirror symmetry (C/M) and no symmetry, respectively. To study the transformation between them, the symmetric connection in PT -antiferromagnet is restricted to P plus C/M . By breaking symmetry with an external field, PT -antiferromagnet can be transformed into altermagnet and fully-compensated ferrimagnet (① and ②), and altermagnet can also be transformed into fully-compensated ferrimagnet (③).

spin-splitting. Altermagnetism and fully-compensated ferrimagnetism not only share certain key properties with antiferromagnetism but also exhibit even more similarities with ferromagnetism. Unlike traditional antiferromagnet, both altermagnet and fully-compensated ferrimagnet can give rise to anomalous Hall/Nernst effect and magneto-optical Kerr effect[5, 10, 11].

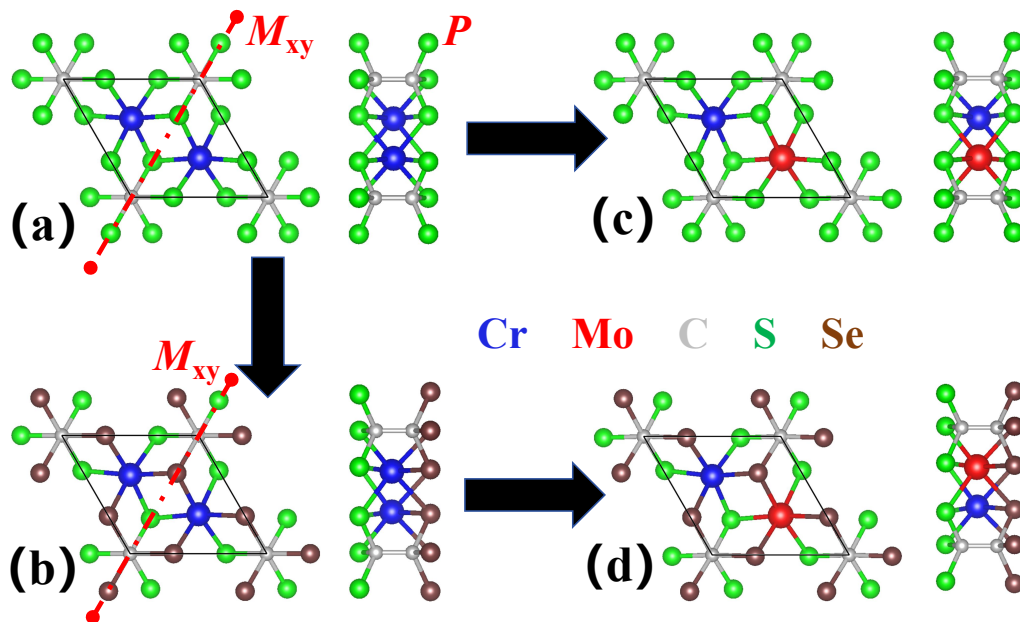


FIG. 2. (Color online) Transitions among crystal structures: the $\text{Cr}_2\text{C}_2\text{S}_6$ (a) can be a parent PT -antiferromagnet with P and M_{xy} symmetries. By Janus engineering, the $\text{Cr}_2\text{C}_2\text{S}_6$ becomes $\text{Cr}_2\text{C}_2\text{S}_3\text{Se}_3$ (b) with M_{xy} symmetry as an altermagnet. By isovalent alloying, the $\text{Cr}_2\text{C}_2\text{S}_6$ and $\text{Cr}_2\text{C}_2\text{S}_3\text{Se}_3$ can become fully-compensated ferrimagnetic CrMoC_2S_6 (c) and $\text{CrMoC}_2\text{S}_3\text{Se}_3$.

The altermagnet exhibits momentum-dependent spin-splitting of d -, g -, or i -wave symmetry in Brillouin zone (BZ) without the help of spin-orbital coupling (SOC)[5, 6, 12–14]. Experimentally and theoretically, several bulk and two-dimensional (2D) altermagnetic materials have been identified that exhibit momentum-dependent spin-splitting[5, 10, 15–20]. Recently, twisted altermagnetism, utilizing one of the five 2D Bravais lattices, has been proposed in twisted magnetic van der Waals (vdW) bilayers[21, 22]. In these systems, an out-of-plane electric field can induce valley polarization due to valley-layer coupling[23, 24]. Additionally, an antiferroelectric altermagnet has been proposed, featuring the coexistence of antiferroelectricity and altermagnetism in a single material[25].

Fully-compensated ferrimagnets constitute a distinctive category of ferrimagnetic materials, marked by their net-zero magnetization[26–28], the spin-splitting of which occurs in the whole BZ with s -wave symmetry, being similar to the situation of ferromagnet. Recently, the significance of 2D fully-compensated ferrimagnets has been increasingly recognized, expanding the realm of low-dimensional spintronic materials[11]. The net-zero magnetization of fully-compensated ferrimagnetism is due to gap-guaranteed spin quantization in one spin channel[11], not symmetry constraints. In our previous works[7, 29–33], CrMoC_2S_6 , $\text{V}_2\text{F}_7\text{Cl}$ and many Janus A-type antiferromagnetic (AFM)-ordering monolayers are strictly 2D fully-compensated ferrimagnets, not antiferromagnets.

Intuitively and vividly elucidating the transitions among these net-zero-magnetization magnets will help

to further reveal the connections of their physical effects and promote their applications in spintronic devices. Here, we start from a parent PT -antiferromagnet to induce altermagnet and fully-compensated ferrimagnet. Based on first-principles calculations, we take parent PT -antiferromagnet CrC_2S_6 monolayer as example to achieve altermagnetic $\text{CrC}_2\text{S}_3\text{Se}_3$ and fully-compensated ferrimagnetic $\text{CrMoC}_2\text{S}_6/\text{CrMoC}_2\text{S}_3\text{Se}_3$ by Janus engineering and isovalent alloying.

Transition among net-zero-magnetization magnets.— From a symmetric point of view[5, 6], the net-zero-magnetization collinear magnets mainly include PT -antiferromagnet, altermagnet and fully-compensated ferrimagnet (see Figure 1), and their magnetic sublattices can be connected by the $[C_2\|P]$, $[C_2\|C/M]$ and the $[C_2\|\text{Null}]$, where C_2 and C/M are the two-fold rotation perpendicular to the spin axis in spin space, and rotation/mirror symmetry in lattice space. To study the transformation between them, the symmetric connection of two sublattices in PT -antiferromagnet is restricted to P plus C/M . The PT -antiferromagnets are spin degenerate due to PT symmetry ($E_\uparrow(k)=PTE_\uparrow(k)=E_\downarrow(k)$), while the altermagnet and fully-compensated ferrimagnet show momentum-dependent (such as d -wave, g -wave and i -wave symmetry) and global (s -wave symmetry) spin-splitting, respectively.

If PT -antiferromagnet is transformed into altermagnet through symmetry breaking, it should possess not only P symmetry but also C/M symmetry. By breaking P symmetry while preserving C/M symmetry, the transformation from PT -antiferromagnet to altermagnet can

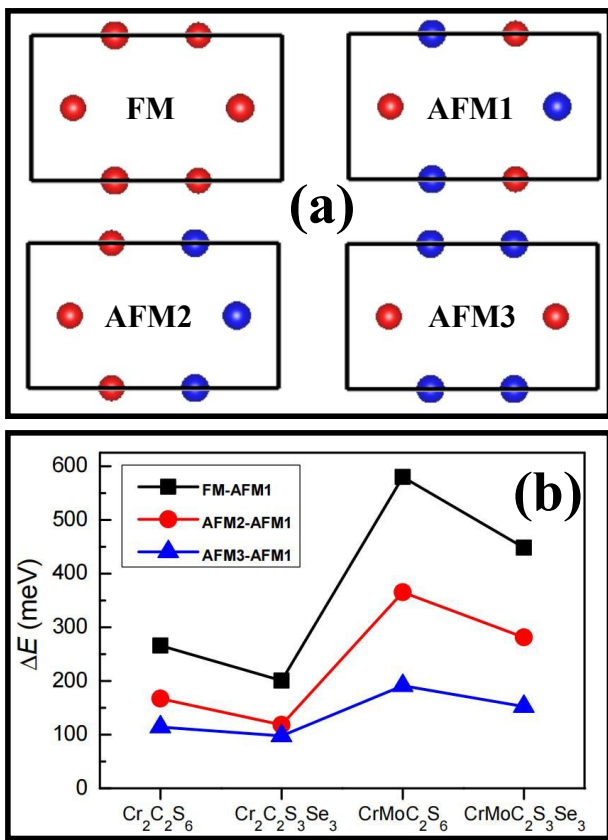


FIG. 3. (Color online) (a): four magnetic configurations, including FM, AFM1, AFM2 and AFM3, and the red and blue balls represent spin-up and spin-down atoms, respectively. (b): the energy differences between FM/AFM2/AFM3 and AFM1 orderings for monolayer Cr₂C₂S₆, Cr₂C₂S₃Se₃, CrMoC₂S₆ and CrMoC₂S₃Se₃.

be achieved (① of Figure 1). To transform from *PT*-antiferromagnet and altermagnet to fully-compensated ferrimagnet, it is only necessary to break both *P* and *C/M* symmetries (② and ③ of Figure 1).

In fact, net-zero-magnetization magnets can be transformed into each other through stacking vdW bilayer engineering. Initially, we take magnetic monolayer as the basic building unit to build the bilayer, where the upper and lower layers can be connected by [*C*₂||*P*] symmetry. By breaking horizontal mirror symmetry of *PT*-bilayer antiferromagnet through a sliding operation, an out-of-plane built-in electric field can be induced[34], which in turn can produce a global spin-splitting, leading to a fully-compensated ferrimagnet. Through twisted-angle engineering[21, 22], the upper and lower layers of *PT*-bilayer antiferromagnet can be connected through rotational symmetry, which can lead to an altermagnet. If an out-of-plane external electric field is applied, *PT*-bilayer antiferromagnet and twisted altermagnet can both become fully-compensated ferrimagnet[23, 30–32]. These reverse processes can be achieved through opposite oper-

ations.

Here, we focus on symmetry-breaking induced transition among net-zero-magnetization magnets. In other words, starting from *PT*-antiferromagnet with the highest symmetry, altermagnet and fully-compensated ferrimagnet are induced through symmetry reduction. Firstly, we search for *PT*-antiferromagnet with *C/M* symmetry by magnetic point group, which can be achieved by high-throughput screening, and then identify more candidates. Secondly, altermagnet and fully-compensated ferrimagnet can be achieved by breaking the corresponding symmetries through electric field, Janus engineering, alloying, defects, and so on. The electric field is a volatile regulation, while the Janus engineering, alloying and defects are non-volatile construction.

Computational detail.— The spin-polarized first-principles calculations are carried out within density functional theory (DFT) [35], as implemented in Vienna ab initio simulation package (VASP)[36–38] by using the projector augmented-wave (PAW) method. We use generalized gradient approximation (GGA) of Perdew, Burke, and Ernzerhof (PBE)[39] as the exchange-correlation functional. The kinetic energy cutoff of 500 eV, total energy convergence criterion of 10⁻⁸ eV, and force convergence criterion of 0.0001 eV.Å⁻¹ are adopted to obtain the reliable results. The Hubbard correction is added with *U*=3.00 eV[40] for *d*-orbitals of both Cr and Mo atoms within the rotationally invariant approach proposed by Dudarev et al[41]. To avoid interlayer interactions, we use a slab model with a vacuum thickness of more than 15 Å along *z* direction. The BZ is sampled with a 13×13×1 Monkhorst-Pack *k*-point meshes for structure relaxation and electronic structure calculations.

The phonon dispersion spectrums are obtained within finite displacement method by using 3×3×1 supercell, as implemented in the Phonopy code[42]. The ab initio molecular dynamics (AIMD) simulations are performed with a 3×3×1 supercell for more than 8000 fs with a time step of 1 fs. The elastic stiffness tensor *C*_{*ij*} are calculated by using strain-stress relationship, and they are renormalized by *C*_{*ij*}^{2D}=*L*_{*z*}*C*_{*ij*}^{3D} with the *L*_{*z*} being the length of unit cell along *z* direction. The magnetic orientation is determined by calculating magnetic anisotropy energy (MAE): *E*_{MAE} = *E*_{SOE}^{||} - *E*_{SOE}[⊥], where || and ⊥ mean that spins lie in the plane and out-of-plane. The Berry curvatures can be calculated from wave functions based on Fukui’s method[43] by using the VASPBERRY code[44–46].

Material realization.— Here, we take monolayer Cr₂C₂S₆ as a prototype example to illustrate symmetry-breaking induced transition among net-zero-magnetization magnets. As shown in Figure 2 (a), the Cr atoms in Cr₂C₂S₆ are surrounded by six S atoms, forming a honeycomb lattice, and two CrS₃ moieties are

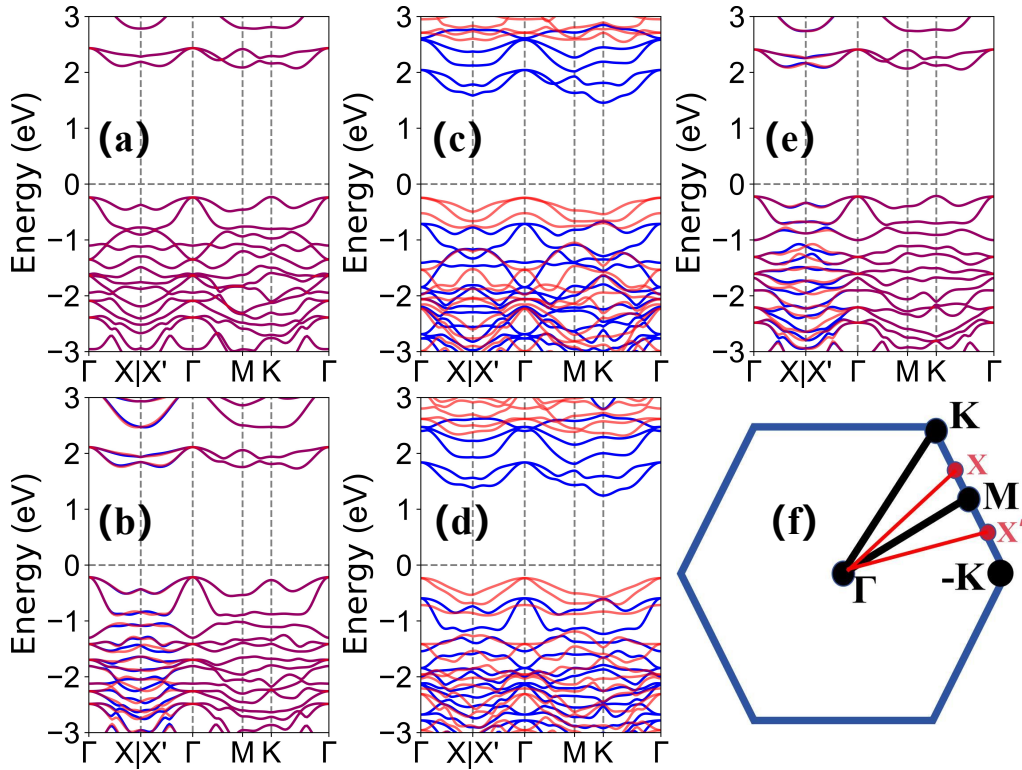


FIG. 4. (Color online) The spin-polarized energy band structures of $\text{Cr}_2\text{C}_2\text{S}_6$ (a), $\text{Cr}_2\text{C}_2\text{S}_3\text{Se}_3$ (b), CrMoC_2S_6 (c), $\text{CrMoC}_2\text{S}_3\text{Se}_3$ (d) and $\text{Cr}_2\text{C}_2\text{S}_6$ at $E=0.30\text{V}/\text{\AA}$ (e) along with BZ with high symmetry points (f). In (a, b, c, d, e), the spin-up and spin-down channels are depicted in blue and red, and the purple color means spin degeneracy.

connected by two C atoms. The $\text{Cr}_2\text{C}_2\text{S}_6$ crystallizes in the $P\bar{3}1m$ space group (No.162), possessing P and M_{xy} symmetries. By replacing the top S layer with Se element in $\text{Cr}_2\text{C}_2\text{S}_6$, the Janus monolayer $\text{Cr}_2\text{C}_2\text{S}_3\text{Se}_3$ is obtained (Figure 2 (b)), which has the symmetry of $P\bar{3}1m$ (No.157). The $\text{Cr}_2\text{C}_2\text{S}_3\text{Se}_3$ lacks P symmetry but still maintains M_{xy} symmetry, which provides the fundamental condition for achieving altermagnet. The $\text{CrMoC}_2\text{S}_6/\text{CrMoC}_2\text{S}_3\text{Se}_3$ (see Figure 2 (c)/(d)) can be obtained by substituting one Cr of $\text{Cr}_2\text{C}_2\text{S}_6/\text{Cr}_2\text{C}_2\text{S}_3\text{Se}_3$ with Mo via isovalent alloying, which crystallizes in the $P\bar{3}12/P\bar{3}$ space group (No.149/No.143), lacking both P and M_{xy} symmetries as fully-compensated ferrimagnet.

To determine the magnetic ground state of the four monolayers, four magnetic configurations, including ferromagnetic (FM), AFM1, AFM2 and AFM3 orderings, have been constructed, as displayed in Figure 3 (a). The energy differences between FM/AFM2/AFM3 and AFM1 orderings are plotted in Figure 3 (b). For all cases, the energy difference is positive, indicating that AFM1 ordering is the magnetic ground state of the four monolayers. The AFM1 ordering, along with the same magnetic ordering of the four monolayers, provides the fundamental condition and convenience for studying the transformation among net-zero-magnetization magnets. Within AFM1 ordering, the optimized equilibrium lat-

tice constants are $a=b=5.636, 5.808, 5.714$ and 5.883 \AA for monolayer $\text{Cr}_2\text{C}_2\text{S}_6, \text{Cr}_2\text{C}_2\text{S}_3\text{Se}_3, \text{CrMoC}_2\text{S}_6$ and $\text{CrMoC}_2\text{S}_3\text{Se}_3$.

To explore the stabilities of four monolayers, the phonon dispersion, AIMD and elastic constants are carried out by using GGA+ U for AFM1 ordering. The calculated phonon spectrums of four monolayers are plotted in FIG.S1[47], and they show no obvious imaginary frequencies, indicating their dynamic stabilities. The total energy as a function of simulation time and the final crystal structure at 8 ps are shown in FIG.S2[47] using AIMD at 300 K, which show that the thermal-induced energy fluctuations and changes in geometry are small, indicating that the four monolayers have good thermal stabilities at 300 K. For monolayer $\text{Cr}_2\text{C}_2\text{S}_6/\text{Cr}_2\text{C}_2\text{S}_3\text{Se}_3/\text{CrMoC}_2\text{S}_6/\text{CrMoC}_2\text{S}_3\text{Se}_3$, the independent elastic constants are $C_{11}=98.83/90.16/91.69/84.42$ Nm^{-1} , $C_{12}=29.56/28.31/34.57/32.36$ Nm^{-1} , and they all satisfy the Born criteria of mechanical stability[48]: $C_{11} > 0$ and $C_{11} - C_{12} > 0$, confirming thier mechanical stabilities.

Without including SOC, the spin-polarized energy band structures of $\text{Cr}_2\text{C}_2\text{S}_6, \text{Cr}_2\text{C}_2\text{S}_3\text{Se}_3, \text{CrMoC}_2\text{S}_6$ and $\text{CrMoC}_2\text{S}_3\text{Se}_3$ are plotted in Figure 4 (a, b, c, d). To clearly observe the altermagnetic spin-splitting, we have

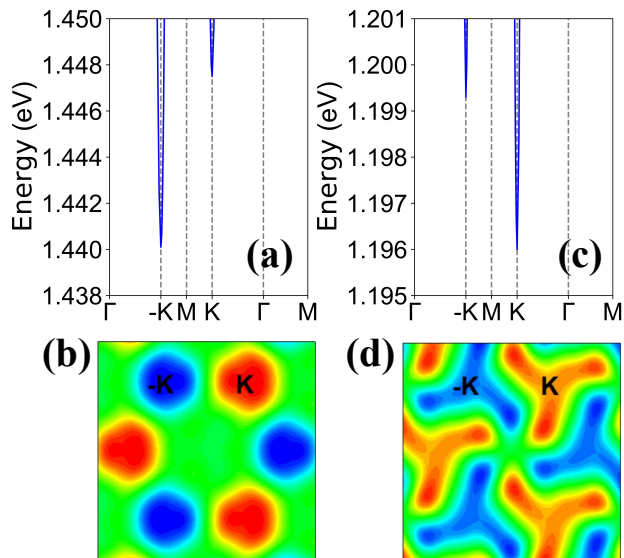


FIG. 5. (Color online) The enlarged energy band structures of conduction bands near the Fermi energy level and the distribution of Berry curvatures of CrMoC_2S_6 (a, b) and $\text{CrMoC}_2\text{S}_3\text{Se}_3$ (c, d) within SOC. In (b, d), the green and red colors represent positive and negative values, respectively.

added the Γ -X|X'- Γ path, which is shown in Figure 4 (f). Due to PT symmetry, $\text{Cr}_2\text{C}_2\text{S}_6$ exhibits spin degeneracy throughout the entire BZ, and it is an indirect bandgap semiconductor with a gap value of 2.31 eV. The total magnetic moment of $\text{Cr}_2\text{C}_2\text{S}_6$ is strictly equal to $0 \mu_B$, with the magnetic moments of the two magnetic atoms being $2.983 \mu_B$ and $-2.983 \mu_B$, respectively.

By Janus engineering, a built-in electric field (about $1.02 \text{ V}/\text{\AA}$ in FIG.S3[47]) in $\text{Cr}_2\text{C}_2\text{S}_3\text{Se}_3$ breaks the PT symmetry, but preserves the mirror symmetry, giving rise to altermagnetic spin-splitting in energy bands. In the absence of the SOC, the symmetry of $\text{Cr}_2\text{C}_2\text{S}_3\text{Se}_3$ possesses a sixfold rotation, leading to spin-splitting of i -wave symmetry. The $\text{Cr}_2\text{C}_2\text{S}_3\text{Se}_3$ is also an indirect bandgap semiconductor of 1.947 eV. The total magnetic moment of $\text{Cr}_2\text{C}_2\text{S}_3\text{Se}_3$ is strictly equal to $0 \mu_B$, and the magnetic moments of two Cr atoms are $3.067 \mu_B$ and $-3.067 \mu_B$, respectively. A built-in electric field can be equivalently replaced by external electric field E , and the spin-polarized energy band structures of $\text{Cr}_2\text{C}_2\text{S}_6$ at $E=0.30 \text{ V}/\text{\AA}$ are plotted in Figure 4 (e), which shows a similar altermagnetic spin-splitting with that of $\text{Cr}_2\text{C}_2\text{S}_3\text{Se}_3$. Its total magnetic moment is still equal to $0 \mu_B$, and the magnetic moments of two Cr atoms are $2.988 \mu_B$ and $-2.988 \mu_B$, respectively. When the direction of the electric field is reversed, the order of spin-splitting also reverses (see FIG.S4[47]), which is feasible for tuning the spin current in spintronic devices.

By isovalent alloying in $\text{Cr}_2\text{C}_2\text{S}_6$ and $\text{Cr}_2\text{C}_2\text{S}_3\text{Se}_3$, both P and M_{xy} symmetries can be broken, which leads to the magnetic atoms with opposite spins being con-

nected asymmetrically in CrMoC_2S_6 and $\text{CrMoC}_2\text{S}_3\text{Se}_3$, producing fully-compensated ferrimagnetic spin-splitting of s -wave symmetry. The large spin-splitting around the Fermi energy level is due to d orbital mismatch between Cr and Mo magnetic atoms[7]. Both CrMoC_2S_6 and $\text{CrMoC}_2\text{S}_3\text{Se}_3$ are indirect bandgap semiconductors, with bandgaps of 1.702 eV and 1.479 eV, respectively. The total magnetic moment of $\text{CrMoC}_2\text{S}_6/\text{CrMoC}_2\text{S}_3\text{Se}_3$ is strictly equal to $0 \mu_B$, and the magnetic moments of the Cr and Mo atoms are $2.892/2.985 \mu_B$ and $-2.355/-2.406 \mu_B$. The different absolute values of the magnetic moments of Cr and Mo atoms with opposite spin polarization are due to their asymmetric connections. From CrMoC_2S_6 to $\text{CrMoC}_2\text{S}_3\text{Se}_3$, the Γ -X and X'- Γ paths will become inequivalent due to the symmetry reduction, leading to the lack of symmetry in the band structure (see FIG.S5[47]).

Achieving valley polarization and the anomalous valley Hall effect (AVHE) in net-zero-magnetization magnets is of great significance for the development of valleytronics devices. Valley polarization can exist in hexagonal PT -antiferromagnet[30, 31]. To achieve AVHE, there should be spin-splitting, which requires breaking the PT symmetry, thus transforming into fully-compensated ferrimagnet. For twisted altermagnet, valley polarization can be induced by an external out-of-plane electric field[23, 24], which in fact transforms it into fully-compensated ferrimagnet. Therefore, fully-compensated ferrimagnet is a natural material for realizing the AVHE. Firstly, we determine the magnetization directions of fully-compensated ferrimagnetic CrMoC_2S_6 and $\text{CrMoC}_2\text{S}_3\text{Se}_3$ by calculating MAE, because only out-of-plane magnetization can produce spontaneous valley polarization[30, 31]. The calculated MAE is $148/209 \mu\text{eV}/\text{unit cell}$ for $\text{CrMoC}_2\text{S}_6/\text{CrMoC}_2\text{S}_3\text{Se}_3$, which means the out-of-plane easy magnetization axis.

The energy band structures of $\text{CrMoC}_2\text{S}_6/\text{CrMoC}_2\text{S}_3\text{Se}_3$ with SOC are plotted in FIG.S6[47], and the enlarged energy band structures of conduction bands near the Fermi energy level and the distribution of Berry curvatures ($\Omega(k)$) are shown in Figure 5. Based on Figure 5 (a, c), it is clearly seen that there exists valley polarization. The energy of K valley of CrMoC_2S_6 is higher than one of -K valley with the valley splitting of 7.4 meV ($|\Delta E_C| = |E_K^C - E_{-K}^C|$). However, for $\text{CrMoC}_2\text{S}_3\text{Se}_3$, the energy of -K valley is higher than one of K valley with the $|\Delta E_C|$ of 3.3 meV. It is clearly seen that the Berry curvatures of the -K and K valleys have opposite signs. When a longitudinal in-plane electric field E_{\parallel} is applied, the Bloch carriers will acquire an anomalous transverse velocity $v_{\perp} \sim E_{\parallel} \times \Omega(k)$ [49]. When the Fermi energy level is shifted between the -K and K valleys in the conduction band of $\text{CrMoC}_2\text{S}_6/\text{CrMoC}_2\text{S}_3\text{Se}_3$, the spin-up carriers from -K/K valley will accumulate along one edge of the sample, giving rise to the AVHE (FIG.S7[47]).

Conclusion.— In summary, we present the transition among net-zero-magnetization magnets, including PT -antiferromagnet, altermagnet and fully-compensated ferrimagnet. From the parent material PT -antiferromagnet, altermagnet and fully-compensated ferrimagnet can be derived through symmetry breaking. Specifically, the parent PT -antiferromagnet possesses initial symmetries P and C/M . Through the process of symmetry breaking, materials with different symmetry of spin-splitting, altermagnet and fully-compensated ferrimagnet, can be induced. This symmetry breaking can be achieved through various methods, such as Janus engineering, isovalent alloying, and external electric field. Through first-principles calculations, we start from PT -antiferromagnetic $\text{Cr}_2\text{C}_2\text{S}_6$ and induce altermagnetic $\text{Cr}_2\text{C}_2\text{S}_3\text{Se}_3$ and fully-compensated ferrimagnetic $\text{CrMoC}_2\text{S}_6/\text{CrMoC}_2\text{S}_3\text{Se}_3$ via Janus engineering and isovalent alloying, and the four monolayers exhibit good stabilities. This research provides valuable insights into transitions among net-zero-magnetization magnets, and gives an intuitive understanding of the underlying mechanisms that govern their magnetic electronic structures.

This work is supported by Natural Science Basis Research Plan in Shaanxi Province of China (2021JM-456). We are grateful to Shanxi Supercomputing Center of China, and the calculations were performed on TianHe-2.

* sandongyuwang@163.com

- [1] S. A. Wolf, D. D. Awschalom, R. A. Buhrman, J. M. Daughton, S. von Molnr, M. L. Roukes, A. Y. Chtchelkanova and D. M. Treger, Spintronics: A Spin-Based Electronics Vision for the Future, *Science* **294**, 1488 (2001).
- [2] X. Hu, Half-metallic antiferromagnet as a prospective material for spintronics, *Adv. Mater.* **24**, 294 (2012).
- [3] T. Jungwirth, X. Marti, P. Wadley and J. Wunderlich, Antiferromagnetic spintronics, *Nat. Nanotechnol.* **11**, 231 (2016).
- [4] T. Jungwirth, J. Sinova, A. Manchon, X. Marti, J. Wunderlich and C. Felsner, The multiple directions of antiferromagnetic spintronics, *Nat. Phys.* **14**, 200 (2018).
- [5] L. Šmejkal, J. Sinova and T. Jungwirth, Beyond conventional ferromagnetism and antiferromagnetism: A phase with nonrelativistic spin and crystal rotation symmetry, *Phys. Rev. X* **12**, 031042 (2022).
- [6] I. Mazin, Altermagnetism—a new punch line of fundamental magnetism, *Phys. Rev. X* **12**, 040002 (2022).
- [7] S. D. Guo, Y. L. Tao, G. Wang and Y. S. Ang, How to produce spin-splitting in antiferromagnetic materials, *J. Phys.: Condens. Matter* **36**, 215804 (2024).
- [8] I. Mazin, R. González-Hernández and L. Šmejkal, Induced Monolayer Altermagnetism in $\text{MnP}(\text{S}, \text{Se})_3$ and FeSe , arXiv:2309.02355 (2023).
- [9] P. Zhou, X. N. Peng, Y. Z. Hu, B. R. Pan, S. M. Liu, Pengbo Lyu and L. Z. Sun, Transition from Antiferromagnetism to Altermagnetism: Symmetry-Breaking Theory, arXiv:2410.17747 (2024).
- [10] L. Bai, W. Feng, S. Liu, L. Šmejkal, Y. Mokrousov, and Y. Yao, Altermagnetism: Exploring New Frontiers in Magnetism and Spintronics, *Adv. Funct. Mater.* 2409327 (2024).
- [11] Y. Liu, S. D. Guo, Y. Li and C. C. Liu, Two-dimensional fully-compensated Ferrimagnetism, under review (2024).
- [12] S. Hayami, Y. Yanagi and H. Kusunose, Momentum-Dependent Spin Splitting by Collinear Antiferromagnetic Ordering, *J. Phys. Soc. Jpn.* **88**, 123702 (2019).
- [13] S. Hayami, Y. Yanagi and H. Kusunose, Bottom-up design of spin-split and reshaped electronic band structures in antiferromagnets without spin-orbit coupling: Procedure on the basis of augmented multipoles, *Phys. Rev. B* **102**, 144441 (2020).
- [14] S. Hayami and H. Kusunose, Essential role of the anisotropic magnetic dipole in the anomalous Hall effect, *Phys. Rev. B* **103**, L180407 (2021).
- [15] S. D. Guo, X. S. Guo and G. Wang, Valley polarization in two-dimensional tetragonal altermagnetism, *Phys. Rev. B* **110**, 184408 (2024).
- [16] H.-Y. Ma, M. L. Hu, N. N. Li, J. P. Liu, W. Yao, J. F. Jia and J. W. Liu, Multifunctional antiferromagnetic materials with giant piezomagnetism and noncollinear spin current, *Nat. Commun.* **12**, 2846 (2021).
- [17] S.-D. Guo, X.-S. Guo, K. Cheng, K. Wang, and Y. S. Ang, Piezoelectric altermagnetism and spin-valley polarization in Janus monolayer Cr_2SO , *Appl. Phys. Lett.* **123**, 082401 (2023).
- [18] X. Chen, D. Wang, L. Y. Li and B. Sanyal, Giant spin-splitting and tunable spin-momentum locked transport in room temperature collinear antiferromagnetic semimetallic CrO monolayer, *Appl. Phys. Lett.* **123**, 022402 (2023).
- [19] Y. Zhu, T. Chen, Y. Li, L. Qiao, X. Ma, C. Liu, T. Hu, H. Gao and W. Ren, Multipiezo Effect in Altermagnetic V_2SeTeO Monolayer, *Nano Lett.* **24**, 472 (2024).
- [20] Y. Wu, L. Deng, X. Yin, J. Tong, F. Tian and X. Zhang, Valley-Related Multipiezo Effect and Noncollinear Spin Current in an Altermagnet $\text{Fe}_2\text{Se}_2\text{O}$ Monolayer, *Nano Lett.* **24**, 10534 (2024).
- [21] Y. Liu, J. Yu and C. C. Liu, Twisted Magnetic Van der Waals Bilayers: An Ideal Platform for Altermagnetism, *Phys. Rev. Lett.* **133**, 206702 (2024).
- [22] R. He, D. Wang, N. Luo, J. Zeng, K. Q. Chen and L. M. Tang, Nonrelativistic Spin-Momentum Coupling in Antiferromagnetic Twisted Bilayers, *Phys. Rev. Lett.* **130**, 046401 (2023).
- [23] S. D. Guo, Y. Liu, J. Yu and C. C. Liu, Valley polarization in twisted altermagnetism, *Phys. Rev. B* **110**, L220402 (2024).
- [24] R. W. Zhang, C. X. Cui, R. Z. Li, J. Y. Duan, L. Li, Z. M. Yu and Y. G. Yao, Predictable gate-field control of spin in altermagnets with spin-layer coupling, *Phys. Rev. Lett.* **133**, 056401 (2024).
- [25] X. Duan, J. Zhang, Z. Zhang, I. Žutić and T. Zhou, Antiferroelectric Altermagnets: Antiferroelectricity Alters Magnets, arXiv:2410.06071 (2024).
- [26] H. van Leuken and R. A. de Groot, Half-Metallic Antiferromagnets, *Phys. Rev. Lett.* **74**, 1171 (1995).
- [27] H. Akai and M. Ogura, Half-Metallic Diluted Antiferromagnetic Semiconductors, *Phys. Rev. Lett.* **97**, 026401 (2006).
- [28] S. Wurmehl, H. C. Kandpal, G. H. Fecher, and C.

- Felsler, Valence electron rules for prediction of half-metallic compensated-ferrimagnetic behaviour of Heusler compounds with complete spin polarization, *J. Phys.: Condens. Matter* **18**, 6171 (2006).
- [29] S. D. Guo and Y. S. Ang, Spontaneous spin splitting in electric potential difference antiferromagnetism, *Phys. Rev. B* **108**, L180403 (2023).
- [30] S. D. Guo, Y. L. Tao, Z. Y. Zhuo, G. Zhu and Y. S. Ang, Electric-field-tuned anomalous valley Hall effect in A-type hexagonal antiferromagnetic monolayers, *Phys. Rev. B* **109**, 134402 (2024).
- [31] S. D. Guo, L. Zhang, Y. Zhang, P. Li and G. Wang, Large spontaneous valley polarization and anomalous valley Hall effect in antiferromagnetic monolayer Fe_2CF_2 , *Phys. Rev. B* **110**, 024416 (2024).
- [32] S. D. Guo, W. Xu, Y. Xue, G. Zhu and Y. S. Ang, Layer-locked anomalous valley Hall effect in a two-dimensional A-type tetragonal antiferromagnetic insulator, *Phys. Rev. B* **109**, 134426 (2024).
- [33] D. C. Liang, S. D. Guo and S. Chen, Anomalous valley Hall effect in electric-potential-difference antiferromagnetic Cr_2CHCl monolayer, *Appl. Phys. Lett.* **125**, 242402 (2024).
- [34] T. Zhang, X. L. Xu, B. B. Huang, Y. Dai, L. Z. Kou and Y. D. Ma, Layer-polarized anomalous Hall effects in valleytronic van der Waals bilayers, *Mater. Horiz.* **10**, 483 (2023).
- [35] P. Hohenberg and W. Kohn, Inhomogeneous Electron Gas, *Phys. Rev.* **136**, B864 (1964); W. Kohn and L. J. Sham, Self-Consistent Equations Including Exchange and Correlation Effects, *Phys. Rev.* **140**, A1133 (1965).
- [36] G. Kresse, Ab initio molecular dynamics for liquid metals, *J. Non-Cryst. Solids* **193**, 222 (1995).
- [37] G. Kresse and J. Furthmüller, Efficiency of ab-initio total energy calculations for metals and semiconductors using a plane-wave basis set, *Comput. Mater. Sci.* **6**, **15** (1996).
- [38] G. Kresse and D. Joubert, From ultrasoft pseudopotentials to the projector augmented-wave method, *Phys. Rev. B* **59**, 1758 (1999).
- [39] J. P. Perdew, K. Burke and M. Ernzerhof, Generalized gradient approximation made simple, *Phys. Rev. Lett.* **77**, 3865 (1996).
- [40] P. Wang, D. X. Wu, K. Zhang and X. J. Wu, Two-Dimensional Quaternary Transition Metal Sulfide CrMoA_2S_6 (A = C, Si, or Ge): A Bipolar Antiferromagnetic Semiconductor with a High Neel Temperature, *J. Phys. Chem. Lett.* **13**, 3850 (2022).
- [41] S. L. Dudarev, G. A. Botton, S. Y. Savrasov, C. J. Humphreys, and A. P. Sutton, Electron-energy-loss spectra and the structural stability of nickel oxide: An LSDA+U study, *Phys. Rev. B* **57**, 1505 (1998).
- [42] A. Togo, F. Oba and I. Tanaka, First-principles calculations of the ferroelastic transition between rutile-type and CaCl_2 -type SiO_2 at high pressures, *Phys. Rev. B* **78**, 134106 (2008).
- [43] T. Fukui, Y. Hatsugai and H. Suzuki, Chern numbers in discretized Brillouin zone: efficient method of computing (spin) Hall conductances, *J. Phys. Soc. Japan.* **74**, 1674 (2005).
- [44] H. J. Kim, <https://github.com/Infant83/VASPBERRY>, (2018).
- [45] H. J. Kim, C. Li, J. Feng, J.-H. Cho, and Z. Zhang, Competing magnetic orderings and tunable topological states in two-dimensional hexagonal organometallic lattices, *Phys. Rev. B* **93**, 041404(R) (2016).
- [46] S. W. Kim, H. J. Kim, S. Cheon and T. H. Kim, Circular dichroism of emergent chiral stacking orders in quasi-one-dimensional charge density waves, *Phys. Rev. Lett.* **128**, 046401 (2022).
- [47] See Supplemental Material at [] for phonon dispersion and AIMD results; the plane-averaged electrostatic potential; the related energy band structures; the schematic diagram of the AVHE .
- [48] R. C. Andrew, R. E. Mapasha, A. M. Ukpong and N. Chetty, *Phys. Rev. B* **85**, 125428 (2012).
- [49] D. Xiao, M. C. Chang and Q. Niu, *Rev. Mod. Phys.* **82**, 1959 (2010).